Journal of Interfaces, Thin films, and Low dimensional systems 7 (2) Winter and Spring (2024) 765-772

The effects of Graphite and CNTs doping on TiO_2 properties in anatase phase

Scientific research paper

Sedigheh Dadras*, Fatemeh Keramatiradmousa

Department of Condensed Matter Physics, Faculty of Physics, Alzahra University, Tehran, Iran

ARTICLE INFO

Article history:
Received 23 November 2023
Revised 12 February 2024
Accepted 26 February 2024
Available online 22 March 2024

Keywords
Titanium dioxide
Carbon nanotubes
Conductivity
Capacitance
Band gap energy

ABSTRACT

In this research, we synthesized titanium dioxide (TiO_2) nanoparticles by sol-gel method, and doped with different percentages (0.2%wt and 0.5%wt) of graphite and carbon nanotubes (CNTs). The X-ray diffraction analysis of the samples showed the formation of anatase phase of pure and doped TiO_2 samples. We checked the morphology and grains size of the samples by using FESEM analysis we measured the grain size, which was reduced from 65 nm to 42 nm by doping. The electrical properties of the samples have investigated by LCR meter and measured the capacitance, energy dissipation, and conductivity of the samples. The results of the electrical measurements showed that the conductivity of the samples increased from 58.51$(\Omega m)^{-1}(*10^{-12})$ to 67.52 $(\Omega m)^{-1}(*10^{-12})$ with doping. We used UV-Vis and FT-IR analysis to investigate optical properties of the samples. We found that CNTs doped samples have more conductivity and smaller grain size than graphite doped samples.

1 Introduction

Titanium dioxide (TiO_2) has emerged as a frontrunner among metal oxide materials due to its remarkable versatility and applicability across a wide range of domains. Its exceptional stability, favorable physicochemical properties, abundant availability, and cost-effectiveness make it a highly sought-after material in diverse fields, including gas sensors [1], lithium-ion batteries [2], renewable energy conversion systems [3] and photocatalysis [4,5]. TiO_2 exists in three natural crystalline forms: rutile, anatase and brookite. The crystalline lattice of rutile and anatase is the tetragonal and the crystalline lattice of brookite is the orthorhombic, rutile and anatase are the most existence in nature and they are easier synthesis than brookite [6]. Titanium dioxide (TiO_2) is a versatile material with a wide range of applications, including photocatalysis, gas sensing, and energy storage [7]. The fundamental building block of TiO_2 is a TiO_6 octahedron, where a single titanium atom is surrounded by six oxygen atoms in an octahedral arrangement. Among the various TiO_2 crystal structures, anatase has been recognized as the most active photocatalyst, despite having a higher bandgap energy compared to other forms of TiO_2 [8].

CNTs have attracted significant research interest in the recent years. CNTs are suitable and economical material for producing highly impressive, effective, miniaturized, and multifunctional devices, because of their high aspect ratios, excellent mechanical stability and physical properties [9]. Among these, the method of doping TiO_2 with carbon compounds such as Graphite, CNTs, Graphene, etc, has been given extensive attention [10]. Graphene is a single-atom-thick material composed of sp2-bonded carbon atoms arranged in a honeycomb lattice. It exhibits remarkable properties, including exceptionally high thermal conductivity (5000 $W\ m^{-1}\ K^{-1}$), exceptional carrier mobility (200,000 $cm^2\ V^{-1}\ s^{-1}$), an unmatched theoretical specific surface area (2630 $m^2\ g^{-1}$), and remarkable transparency owing to its atomic thickness [11,12]. Combining graphene with TiO_2 has shown promise in enhancing TiO_2's

*Corresponding author.
Email addresses: Dadras@Alzahra.ac.ir
DOI: 10.22051/jitl.2024.45635.1100

photocatalytic performance [10]. In this research, we doped TiO_2 with different percentage of CNTs and graphite to improve the properties of TiO_2 and compared them.

2 Experimental

To synthesize TiO_2 nanoparticles, we chose the sol-gel method because it has more popularity and industrial application than other methods and can produce high-quality nanoparticles (production of particles with the same size). In this method, the first step includes preparing a homogeneous solution. For this step, the solvent that pure ethanol (C_2H_5OH) and the precursor that dissolves titanium tetrachloride ($TiCl_4$) with a purity of 99.99% together to prepare a homogeneous solution. First, 10 ml of pure ethanol (C_2H_5OH) in a 100 ml beaker with a pipette, and following the safety precautions, add 1 ml of $TiCl_4$ to the ethanol slowly and drop by drop under the hood. The magnet was placed in the solution and the beaker containing the solution and the magnet was placed on a magnetic stirrer for 30 minutes to homogenize and form a yellow homogeneous solution. After the homogenization stage, the obtained sol was placed on a magnetic stirrer with an average temperature of 65°C for 1 hour to turn into a gel, and after the formation of the gel, in order to carry out the drying process, the yellow gel was kept for 1 hour. Put it on the heater for 3 hours with an average temperature of 75◦C until the remaining HCl vapors are removed and the gel is completely dry and a white powder is formed. Then, we prepared five 0.5 grams TiO_2 samples with different percentages of graphite and CNT. In this doping, the substrate is TiO_2 and the substance that is added as impurities is CNTs and Graphite. They are pure and 0.2%wt CNT, 0.5%wt CNT, 0.2%wt Graphite, 0.5%wt Graphite doped TiO_2 samples. The pellets were pressed under 8 tons' pressure for a period of 1 hour. To form the anatase phase, all synthesis pellets were placed in a furnace at the same time and heated for 3 hours at 450 ◦C until the anatase phase was formed. The structural analysis and characterization of the samples were performed by X-ray powder diffraction (XRPD), Field Emission Scanning Electron Microscope (FESEM), LCR meter, Ultraviolet Visible Spectrometer (UV-VIS) and Fourier Transform Infrared Spectrometer (FT-IR). Rigaku Ultima IV diffract meter with Cu Kα radiation (λ =1.54178 Å) was employed for the XRPD measurements. The diffraction patterns were recorded in 10 to 80 º range (2θ) at a rate of 0.02 degree on a D/teXUltra high-speed (1D) detector. FESEM observation of the prepared samples was performed by using a Field Emission Scanning Electron Microscope – TESCAN(VEGA//XMU) and it was measured on a scale of 500 nm. The analysis of the LCR meter was performed by the LCR device – PERECISION model 6200 made by Gwinstek. Then Elmer Perkin Lambeda model analyzer was used for UV-Vis analysis and we obtained the UV-Vis spectrum of all samples in the wavelength range of 200 nm to 700 nm. Finally, FT-IR analysis of the samples synthesized in the laboratory was performed using the FT-IR spectrometer of Bruker company laboratory.

3 Results & discussion

X-ray powder diffraction (XRD) patterns were obtained for pure TiO_2, TiO_2/CNTs, and TiO_2/G to investigate their crystalline structures. As shown in Fig. 1, the XRD peaks observed at 2θ angles of ~25.3° (101), ~37.8° (004), ~48.1° (200), ~53.9° (105), ~55.1° (211), ~62.9° (204), ~68.7° (116), ~70.3° (220), and ~75.1° (215) confirmed the formation of the anatase crystalline phase at 450°C [13,14]. According to Debby-Scherrer equation, ($d = k \boldsymbol{\lambda} / \beta \cos\theta$), the crystalline size (d) of the samples was determinded and brought in Table 1. Where, K is a constant (0.94), λ is X-ray wavelength (1.54178 Å), β is the full width at half maximum of the peak considered for calculation (101 and 200) and θ is the angle of the diffraction peak. As it can be seen in Table 1, the crystalline size of the doped samples decreases in respect to the pure sample, while the average size of the crystals has decreased from 14 nm for pure TiO_2 to about 10 nm in the 0.5%wt CNT doped sample. Figure 2 showed the FE-SEM images of a) pure, b) 0.2%wt graphite doped, c) 0.5%wt graphite doped, d) 0.2%wt CNT doped and e) 0.5%wt CNT doped, TiO_2 samples. The surface morphology of pure TiO_2, as shown in Fig. 2a, is characterized by aggregates with irregular geometric shapes separated by cracks and holes. This porous structure, arising from the presence of cracks and holes, imparts both trans-particle porosity and inter-particle porosity to the material. This porous structure is crucial for TiO_2's photocatalytic performance, as it provides additional surface area for reactant adsorption and enhances the diffusion of reactants and products within the material.

Additionally, the porous structure serves as a stabilizer for embedding and interlocking carbon nanotubes (CNTs) and graphene (G) when creating TiO_2/CNTs and TiO_2/G nanocomposites, further enhancing the photocatalytic activity. The incorporation of CNTs or G also promotes the transfer of photogenerated electrons from TiO_2 to the carbon nanomaterials, reducing electron-hole recombination and improving photocatalytic efficiency. Overall, the surface morphology of TiO_2 plays a significant role in its photocatalytic performance and its ability to form stable nanocomposites with CNTs and G [15]. Using the Digimiser software and by averaging the diameter of 50 grains, the average grain size of pure, doping with graphite (0.2%wt) and (0.5%wt) and doping with CNTs (0.2%wt) and (0.5%wt) TiO_2 were obtained as 65, 53, 50, 48, 42 nm, respectively (Table 1). Decreasing the particle sizes and increasing the surface area to volume of particles, cause an increase in the reactivity of the material [16].

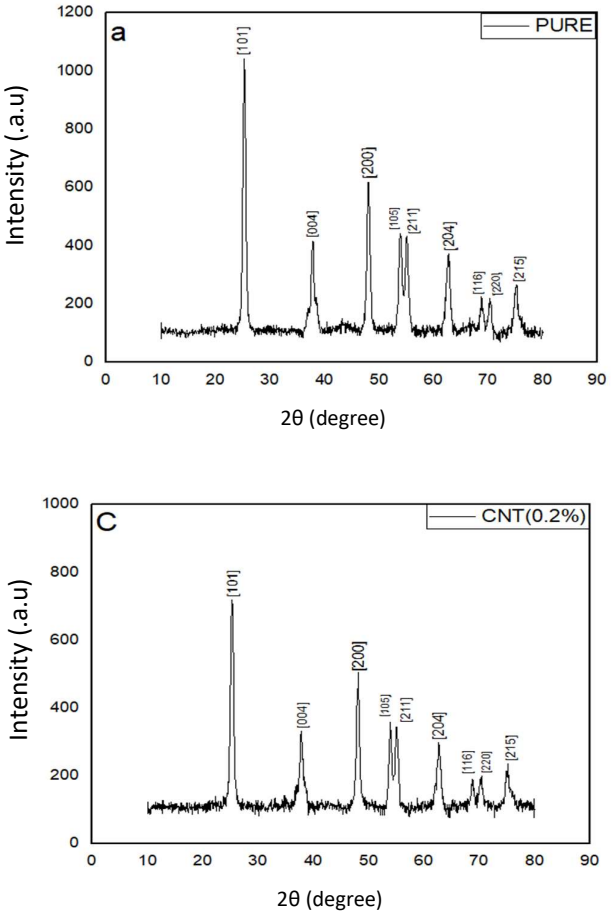

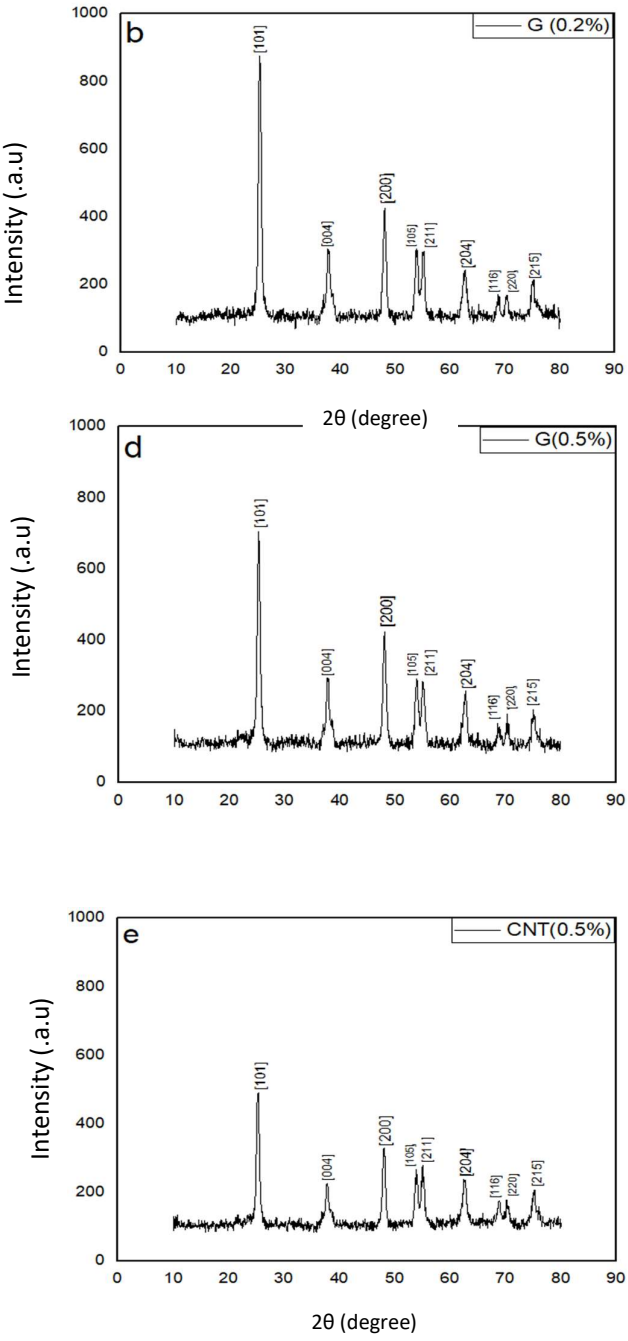

Figure 1. XRPD spectra of, a) pure, b) doped with graphite (0.2%wt), c) doped with CNTs (0.2%wt), d) doped with graphite (0.5%wt), e) doped with CNTs (0.5%wt), TiO_2 sample.

As the particle size decreases, the surface area increases in relation to the volume, which makes TiO_2 contaminated with CNTs have a larger surface area than TiO_2 contaminated with graphite nanoparticles. The reason for this is that the presence of multi-walled carbon nanotubes in nanocomposite coatings prevents the growth of TiO_2 crystals. Grain boundaries act as trap positions in the path of electrons [17].

Table 1: Crystallite size and average grains size of the samples.

Sample	Crystallite size (nm)	Average grains size (nm)
TiO2 (Pure)	14	65
TiO2 / G (0.2%wt)	13	53
TiO2 / G (0.5%wt)	12	50
TiO2 / CNT (0.2%wt)	11	48
TiO2 / CNT (0.5%wt)	10	42

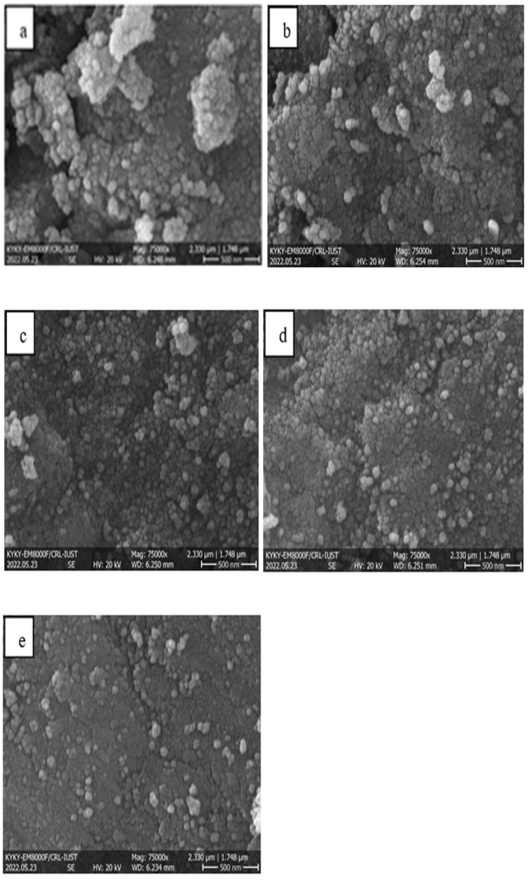

Figure 2. FE-SEM images of a) pure b) 0.2%wt graphite doped c) 0.5%wt graphite doped d) 0.2%wt CNT doped e) 0.5%wt CNT doped TiO_2 samples.

We used UV-Vis analysis to check the optical properties of the samples in the wavelength range of 200 nm to 700 nm. As shown in Fig. 3, in the ultraviolet wavelength (200-400) nanometers, the absorption rate of pure TiO_2 is higher than the other samples because the optical activity of TiO_2 depends on its band gap, the band gap of TiO_2 is in ultraviolet range that is equal to 2.3 (eV) in the anatase phase. By increasing the wavelength and entering the range of visible wavelength (400-700) nm, the absorption rate of pure and doped TiO_2 samples decrease.

By doping pure TiO_2 with different weight percentages of graphite and CNTs, we tried to increase the absorption in the visible wavelength range to increase the use of titanium dioxide for solar cells and photocatalytic devices. According to Fig. 3 the absorption in the visible range wavelength (400-700) nm, the CNTs doped TiO_2 samples have higher absorption rates in the visible range compared to the graphite doped and pure TiO_2.

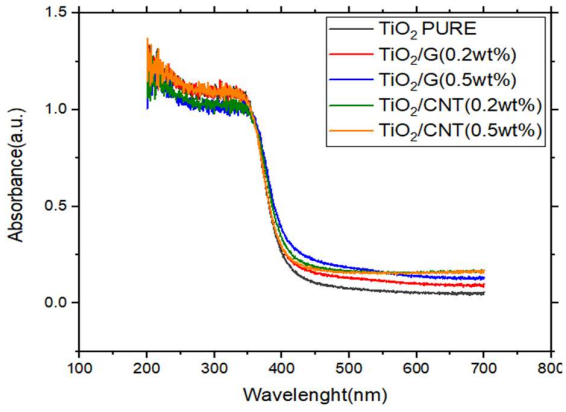

Figure 3. Absorbtion versus UV-Vis wavelenght for all the samples.

Titanium dioxide has a high refractive index and absorption of visible light, as the band gap decreases, the absorption of sunlight increases.

The band gap of TiO_2 in the anatase phase is reported to be about 3.2 eV. To reduce the band gap, TiO_2 can be doped with carbonaceous compounds. We calculated the band gap of pure and doped with graphite and CNTs samples. The band gap was obtained by using the formula [18] as $\alpha h\nu = A (h\nu - E_g)^{n}$ and drawing the curve $(\alpha h\nu)^{1/2}$ in terms of hv for the indirect transition n=2 and from the intersection of the tangent line with the curve. Figure 4 shows the $(\alpha h\nu)^{1/2}$ versus hv of the samples. The band gap for pure sample is 2.90 eV, TiO_2 doped with 0.2%wt and 0.5%wt graphite is 2.88 and 2.80 eV, respectively, and for TiO_2 doped with 0.2%wt

and 0.5%wt CNTs is 2.88 and 2.73 eV respectively. As it is shown in Table 2 the highest band gap reduction is for TiO_2 doped with 0.5%wt CNTs.

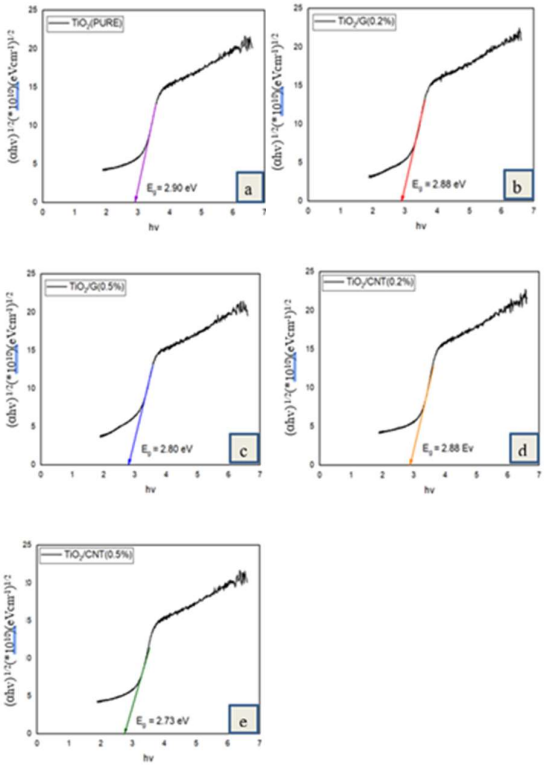

Figure 4. Band gap for a) TiO_2 (pure) b) TiO_2 doped with graphite (0.2%wt) b) TiO_2 doped with graphite (0.5%wt) c) TiO_2 doped with CNTs (0.2%wt) d) TiO_2 doped with CNTs (0.5%wt) samples

Also, reducing the band gap causes an increase in electrical conductivity. Recently, researcher use TiO_2 to increase the electrical conductivity of lithium ion batteries (LIBs) [19], and in order to increase the electrical conductivity and applications of TiO_2, researchers have doped TiO_2 with highly conductive materials [20].

In continue, the electrical properties of the samples are investigated by the LCR meter and the dielectric coefficient, dissipation and conductivity of the samples are determined. By using the relation $\sigma_{ac} = 2\pi f \varepsilon_0 \varepsilon''$, ac electrical conductivity has been calculated that ε_0 is the permittivity of the free space, ε" is imaginary part of the sample permittivity and f is frequency. The results of the electrical measurements showed that the conductivity of the samples increase with doping (Fig. 5a). The increase in electrical conductivity of the sample doped with CNTs (0.5%wt) is higher than the other samples and it is shown in Table 2 that the highest electrical conductivity is for TiO_2 doped with 0.5%wt CNTs.

Permittivity can also be expressed as a complex number

$$\varepsilon(\omega) = \varepsilon'(\omega) + i\varepsilon''(\omega) \quad ,$$

where "ε' and ε are the realand imaginary parts of the elevtrical permitivity. The real part of the permittivity is the dielectric coefficient, that is measured in a physical circuit. The imaginary part expresses the energy dissipation. In circuits, permeability is the second most important parameter that is considered in the design and energy dissipation which is usually more important in the selection of materials. Figure 5 is a comparison of the real (b) and imaginary (c) parts of the sample permeability. The amount of energy dissipation is expressed by the dissipation tangent, tan δ = ε" / ε'. The increase in "ε is smaller than the increase in ε', the dissipation tangent becomes smaller, and this includes a decrease in the amount of energy dissipation. Also, it is shown in Table 2 that the lowest energy dissipation is for TiO_2 doped with 0.5%wt CNTs.

Table 2. Comparison of band gap, electrical conductivity in (50KHz,200KHz) and energy dissipation in (5KHz).

Sample	Band gap (eV)	Electrical conductivity $(\Omega m)^{-1}(*10^{-12})$		Energy dissipation
		50KHz	200KHz	5 KHz
TiO2 (Pure)	2.90	19.71	58.51	0.140
TiO2 / G (0.2%wt)	2.88	16.16	58.31	0.139
TiO2 / G (0.5%wt)	2.80	20.18	59.07	0.129
TiO2 / CNT (0.2%wt)	2.88	21.70	59.86	0.129
TiO2 / CNT (0.5%wt)	2.73	22.37	67.52	0.119

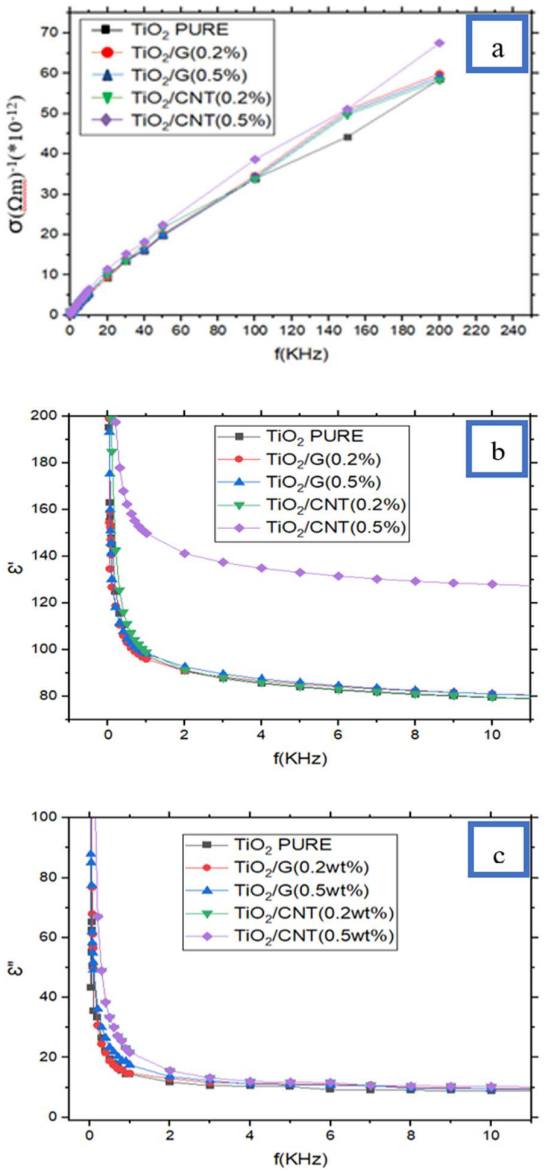

Figure 5. The a) electrical conductivity versus frequency of the samples b) real and, c) imaginary part of the samples permeability vs frequency

Also, using FT-IR analysis, we checked the absorption and transmission of the samples in the infrared spectrum. FT-IR is an analysis used to identify functional groups. This technique draws the intensity of the infrared spectrum based on the absorption wavelength. There are three vibrational bands in Fig. 6 that the vibrational band 495 represents the stretching vibration (Ti-O) while the vibrational band 1638 corresponds to the bending vibrations of the group (-OH) where the 3445 vibrational band corresponds to the stretching vibration (-OH). Also the vibrations in the range of 2800-3800 are the vibrations of bonds (C-H) and (O-H) [21].

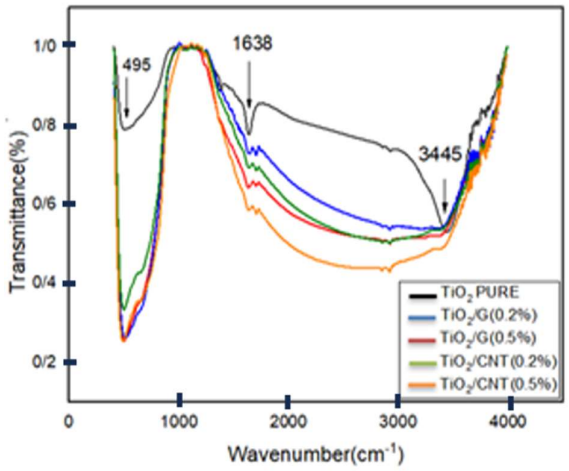

Figure 6. FT-IR analysis spectrum of the samples.

Figure 6 shows that the increase of carbonaceous compounds causes a decrease in the intensity of transmission. The highest transmission intensity is for the pure and the lowest transmission intensity is for the 0.5%wt CNTs doped TiO_2 sample. Therefore, the CNTs doped TiO_2 compound with the highest absorption and the lowest transmission in the infrared spectrum, could be a good option for solar cells application.

4 Conclusions

The presented research was motivated to improve the properties of TiO_2, also produce nanocomposites based on TiO_2 with graphite and CNTs, which can be used for different application, like gas sensors, solar cells, lithium batteries or photocatalysts. According to the obtained results, the following conclusions are drawn:

The results of XRD analysis showed the formation of anatase phase of pure and doped TiO_2 synthesized samples. Also, the crystallite size of the samples decreased by increasing the weight percentage of dopants. FESEM images of the samples show that the average grains of the doped samples decrease by increasing the weight percentage of dopants in compounds. The maximum grain size reduction is for 0.5%wt CNTs doped TiO_2 sample. The UV-Vis absorption spectrum shows an increase in absorption intensity in the visible wavelength region of the doped samples. The highest absorption intensity is for the CNTs doped samples. Also, the energy gap of the doped samples decreased in comparison to the pure one. The 0.5%wt CNTs doped TiO_2 sample has the highest

reduction in the energy gap and maximum conductivity among all the samples. Further, by examining the real and imaginary parts of the dielectric function of the samples, we found that with increasing frequency, the energy dissipation and dielectric constant decrease, and by increasing the dopants the energy dissipation decreases. The results of FT-IR analysis show that by graphite nanoparticles and CNTs doping in TiO_2 compound, the intensity of infrared transmission decreases and so photocatalytic activity can increase. Therefore, the 0.5%wt CNTs doped TiO_2 sample with the highest absorption and lowest transmission intensity is a suitable option for the solar cells and TiO_2 photocatalytic applications [22].

Acknowledgements

This work was financially supported by Alzahra University.

References

[1] Z. M Seeley, A. Bandyopadhyay, S. Bose, "Titanium dioxide thin films for high temperature gas sensors." Thin Solid Films, 519 (2010) 434-438.

[2] T. Ohzuku, Z. Takehara, S. Yoshizawa, "Nonaqueous lithium/titanium dioxide cell." Electrochimica Acta, 24 (1979) 219-222.

[3] S. Y. Wu, W. C. Lu, K. C. Chen, J. L. He, "Study on the preparation of nano-flaky anatase titania layer and their photovoltaic application." Current Applied Physics, 10 (2010) S180-S183.

[4] A. Fujishima, T. N. Rao, D. A. Tryk, "Titanium dioxide photocatalysis." Journal of Photochemistry and Photobiology C: Photochemistry Reviews, **1** (2000) 1-21.

[5] X. Wang, Z. Li, J. Shi, Y. Yu, "One-dimensional titanium dioxide nanomaterials: nanowires, nanorods, and nanobelts." Chemical Reviews, **14** (2014) 9346-9384.

[6] U. Diebold, "The surface science of TiO_2." Surface Science Reports, **48** (2009) 53-229.

[7] L. Stephen., "Titanium Dioxide Versatile Solid Crystalline: An Overview." Assorted Dimensional Reconfigurable Materials, (2020) S35-S36.

[8] J. Zhang et al., "New understanding of the difference of photocatalytic activity among anatase, rutile and brookite TiO_2." Physical Chemistry Chemical Physics, **16** (2014) S20382–S20386.

[9] K. S. Ibrahim, "Carbon nanotubes-properties and applications: A Review." Carbon Letters, **14** (2013) 131e144.

[10] R. Long, N. J. English, O. V. Prezhdo, "Photo-induced charge separation across the graphene-TiO_2 interface is faster than energy losses: A time-domain ab initio analysis." Journal of the American Chemical Society, **134** (2012) 14238–14248.

[11] K. S. Kim, Y. Zhao, H. Jang, S.Y. Lee, J. M. Kim, K. S. Kim, J. H. Ahn, P. Kim, J.Y. Choi, B. H. Hong, "Large-scale pattern growth of graphene films for stretchable transparent electrodes." Nature, **457** (2009) 706–710.

[12] R. R. Nair et al., "Fine structure constant defines visual transparency of graphene." Science, **320** (2008) 1308–1308.

[13] M. Ghadiry et al., "Ultra-sensitive humidity sensor based on optical properties of graphene oxide and nano-anatase TiO_2." PLOS ONE, **11** (2016), e0149593.

[14] S. Wang, X. Cheng. "Solar photocatalytic degradation of typical indoor air pollutants using TiO_2 thin film codoped with iron (III) and nitrogen." Journal of Spectroscopy, **2015** (2015) S1-S6.

[15] P. Paunović,et al., "Structural changes of TiO_2 as a result of CNTs incorporation." Materials Science & Engineering, **6** (2022) 31-39.

[16] Debsish Sarkar, "Nanostructures Ceramics: Characterization and Analysis." CRC Press (2018).

[17] Sada Kasap, "Principles of Electronic Materials and Devices (2nd Edition)." (2006) New York, McGraw-Hill.

[18] A. R. Zanatta, "Revisiting the optical bandgap of semiconductors and the proposal of a unified methodology to its determination." Scientific Reports, **9** (2019) 11225.

[19] Y. F. Yuan et al., "Foam-like, 3-dimension mesoporous N-doped carbon-assembling TiO_2 nanoparticles (P25) as high-performance anode material for lithium-ion batteries." Journal of *Power Sources*, **420** (2019) 38-45.

[20] S. Chattopadhyay, S. Maiti, L. Das, S. Mahanty, G. De, "Electrospun TiO_2-rGO composite nanofibers with ordered mesopores by molecular level assembly: a high performance anode material for lithium-ion batteries." Advanced Materials Interfaces, **3** (2016) 1600761.

[21] Matouke Moise, "FTIR study of the binary effect of titanium dioxide nanoparticles ($nTiO_2$) and copper (Cu^{2+}) on the biochemical constituents of liver tissues of catfish." Toxicology Reports, **6** (2019) 1061-1070.

[22] G. Susana, H. David, C. Jorge, H. Carlos, V. Lizbeth, A. Benjamín, R. Omar, "Development of a low-cost photocatalytic aerogel based on cellulose, carbon nanotubes, and TiO_2 nanoparticles for the degradation of organic dyes." Carbohydrate Polymers, **324** (2024) 121476.